Chapter 3

Technical details

The experiments of this work were performed on two different kinds of samples. One type consisted of lanthanide-metal films grown epitaxially *in situ* on a W(110) substrate crystal. These systems are well-defined and sufficiently simple to allow a detailed data analysis. The second type were films grown *ex situ* by molecular-beam epitaxy (MBE), embedded between Y layers. The samples have different properties and give the opportunity to study the influence of different boundaries on the magnetic structure. Furthermore, Y is a standard material for epitaxial growth of heavy lanthanide metals and is often used to separate magnetic Ho slabs in Ho/Y multilayer systems. This allows the comparison of the results obtained here with data in the literature. Once produced, the second type of samples could be measured using various scattering techniques in different facilities, like conventional x-ray scattering, magnetic soft x-ray scattering, and neutron scattering.

Substrate and sample holder

Lanthanide metals are extremely reactive. Therefore, the preparation of lanthanide-metal films requires *ultra-high vacuum* (UHV) conditions with a residual gas pressure below $1 \cdot 10^{-10}$ mbar. The films were prepared by vapor deposition of high-purity lanthanide metals onto the (110) surface of a tungsten single crystal.

Tungsten (W) is a refractory metal that does not form alloys with lanthanide metals, even up to their desorption temperature. This leads to sharp interfaces between the lanthanide films and the substrate. Lanthanide metals grow as high quality films on W(110) despite a considerable lattice mismatch. The crystalline structure of tungsten is body-centered cubic and thus the (110) surface does not match the symmetry of the hexagonal close-packed planes of the lanthanide metals. Furthermore, there is a mismatch of about 10 to 20 percent between the in-plane parameters of substrate and film. This leads to various superstructures in the submonolayer regime [47]. Nevertheless, the lanthanide-metal films quickly adapt their intrinsic structure; at film thicknesses of more than one monolayer, hexagonal pattern are observed in *low-energy electron diffraction* (LEED) [91].

In order to clean the W surface or to desorb a lanthanide metal film, the crystal has to be 'flashed', i.e. heated by electron bombardment for a few seconds to about 2000 K. Carbon

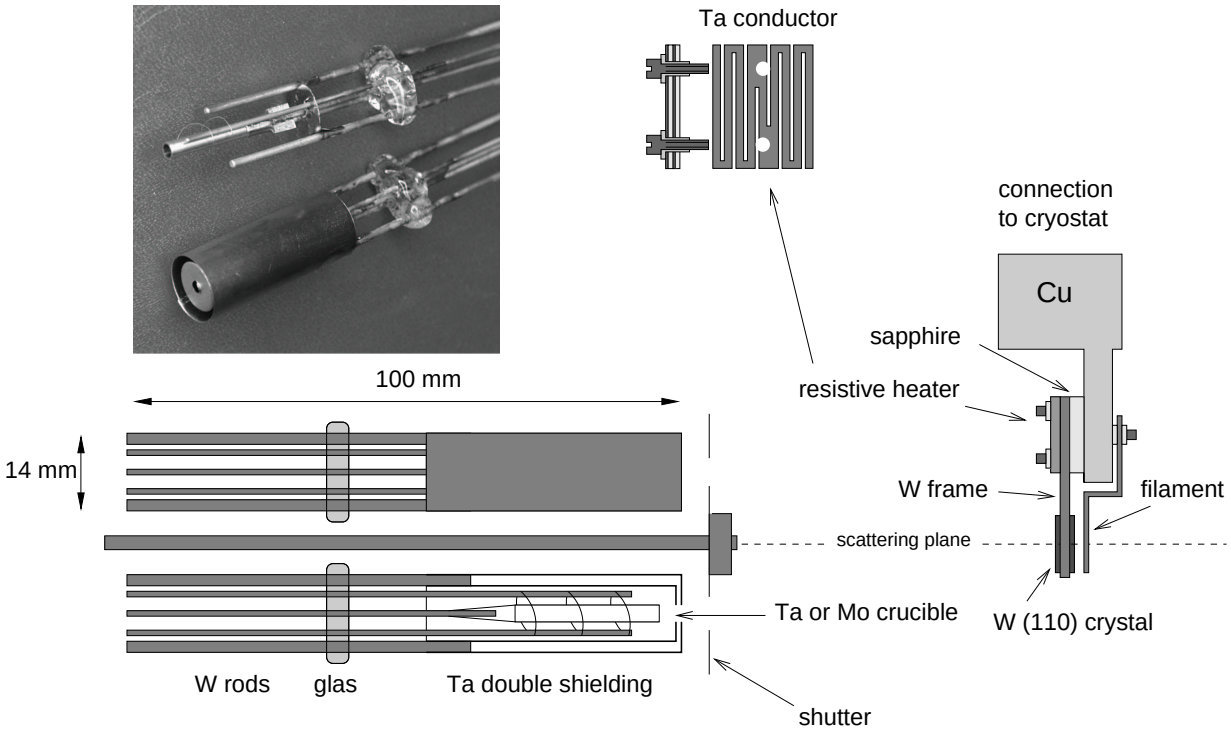

Figure 3.1: Schematic drawing of evaporators (left) and sample holder (right) as used in this work. The arrangement allows to measure the x-ray reflectivity from the sample during evaporation. The small figure on top gives details of the resistive heater. The photograph shows two evaporators, one with and one without Ta shielding.

that segregates from the W bulk successively to the surface is removed by annealing the crystal in oxygen atmosphere. During this procedure, the crystal is held at a temperature of about 1100 K for about 20 minutes, with a partial pressure of oxygen of $1 \cdot 10^{-6}$ mbar in order to oxidize the carbon. Subsequently, the W crystal is flashed to remove the formed tungsten oxide. A clean substrate crystal shows no superstructure in the LEED pattern.

For measurements at low temperatures, the sample holder was mounted on an APD closed-cycle He refrigerator. The experiments require a sample holder that is capable of operating in a temperature interval between 30 K and 300 K for the measurement and up to 2000 K for the cleaning procedure. To cover this wide temperature range, the W crystal is mounted to a Ta or W frame, which is separated by a sapphire plate from the copper cold finger of the refrigerator. At low temperatures, sapphire is a good thermal conductor, allowing an efficient cooling to 30 K. At high temperatures, sapphire shows a poor thermal conductivity and protects the refrigerator from the heat load during flashing and glowing of the substrate.

For temperature-dependent experiments, a filament mounted directly behind the W crystal was used as a heater. While this was useful in case of the conventional x-ray experiments, this setup could not be used in case of soft x-ray experiments, because the visible light from the filament was picked up by the Si-diode photon detector and disturbed

the scattering experiment. In order to avoid visible light from the heater, a radiationless resistive heater was designed. A 0.1-mm-thick Ta plate was cut from two sides to give a meandered conductor (see figure 3.1). The conductor is sandwiched between two 0.5-mm-thick sapphire plates and capped by a Ta plate to shield any residual visible light produced by operating at high power. This heater is small enough to be mounted directly onto the sample holder. A schematic drawing of the sample holder and the heater as used in this work for soft x-ray scattering is displayed on the right side of figure 3.1.

The only temperature sensor available in the required temperature range is a W/Re thermocouple ($W_{0.95}Re_{0.05}/W_{0.74}Re_{0.26}$). Unfortunately, this has a comparably low differential thermopower at low temperatures, where the measurements require high accuracy. For temperature control, we used a commercial *Lakeshore 330* unit with an internal temperature reference. To achieve best thermal contact, the thermocouple wires of 0.125 mm diameter each, stick tightly in a bore of 0.3 mm, machined directly into the W crystal. The whole setup was calibrated carefully as described in reference 90. The error bar in the temperature measurements was determined to be ± 1 K in the temperature range from 100 K to 250 K.

Evaporators

Lanthanide-metal films were prepared by vapor deposition of high purity lanthanide metals (99.99 percent). The metals were vaporized from home-made evaporators with a Ta or Mo crucible (left side of figure 3.1), heated either radiatively or by electron bombardment from a filament wound around the crucible. The crucible and the filament are surrounded by a double Ta shielding, which can also be heated by electron bombardment to reduce contaminations. The evaporators are small in size allowing that nine of them can be mounted onto a CF-64 flange.

To reduce the surface area of the lanthanide-metal pieces they were molten several times in an arc furnace in Ar atmosphere before loading the evaporator. After each run, the surface with the bloated contaminations was cleaned by scraping. Alternatively, the metal pieces were molten in several steps directly in the crucible under *high-vacuum* conditions. After filling and mounting in UHV, the evaporators were carefully degassed at low evaporation rates. With a well-prepared evaporator the pressure during evaporation rises only to $5 \cdot 10^{-10}$ mbar, at most. The evaporation rate and thus the film thickness was controlled by a commercial quartz balance, which can be calibrated very precisely by measuring growth oscillations in the x-ray reflectivity as described in the following section, or by reflectivity measurements of the final film as described in chapter 4.

Growth parameters

One challenging aspect in ultrathin-film research is to find the proper growth parameters for film preparation. The important growth parameters are the evaporation rate, the substrate temperature during growth, the annealing temperature, and the duration of annealing. For different thicknesses, the growth conditions can be quite different. While lanthanide films

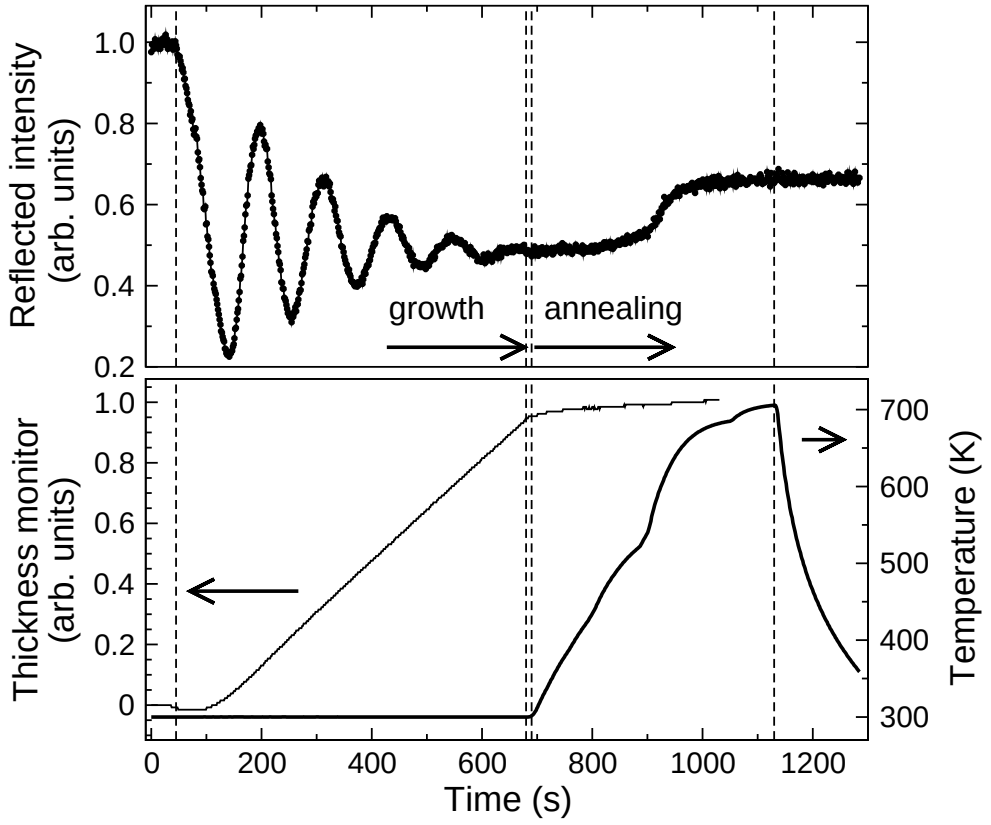

Figure 3.2: Upper panel: growth oscillations during the preparation of a 20-ML Ho film. The intensity was recorded in specular geometry with a momentum transfer of $L = 0.5\,c^*$. In this geometry, one oscillation corresponds to the growth of two double layers. The two curves in the lower panel show the readout from the thickness monitor and the substrate temperature during growth and annealing. After 45 s the shutter was opened, followed by a growth process up to 680 s. The annealing process started after 690 s and ended after 1130 s.

of more than 100 monolayers were grown in two steps with an intermediate annealing of the seed layer and a final annealing to a higher temperature, ultrathin films of only a few monolayers were grown in one step and partly without any annealing.

The growth conditions were found and controlled by different techniques, such as low-energy electron diffraction, photoelectron spectroscopy, and x-ray scattering. In a scattering experiment it is possible to monitor the growth and annealing process directly by monitoring the specular reflectivity. An example of the complete growth process of a 20-ML Ho film is shown in figure 3.2. The upper panel shows the reflected intensity. The substrate temperature and the readout of the thickness monitor during growth and annealing are displayed in the lower panel. The growth oscillations were recorded in a fixed specular scattering geometry with a momentum transfer of $L = 0.5\,c^*$. The high reflectivity at the beginning is that of the clean W substrate held at room temperature. After 45 s the shut-

element	film thickness (atomic layers)	evaporation rate (Å/min)	annealing temperature (K)	duration of annealing (s)
Dy	20 - 22*	1-2*	670*	600-850*
	102 - 320	6-9	800-880	800-2000
	47	3.5	700	900
Ho	110	4.7	700	500 holding 5 min
	10 - 52	5-6	670	400-600 holding 1 min
	11 - 13	1.1	without annealing	-

Table 3.2: Growth parameters of heavy lanthanide-metal films prepared on a W(110) substrate. Dy films thicker than 100 Å were grown in two steps with an intermediate film thickness and intermediate annealing temperature marked with *. All films were deposited with the substrate held at room temperature.

ter in front of the evaporator was opened and damped growth oscillations were observed. The number of oscillations per double layer is given by the inverse length of the scattering vector in reciprocal lattice units [90, 92, 93]. Thus, in the chosen scattering geometry with a momentum transfer of $L = 0.5\,c^*$, there is one growth oscillation per 4 monolayers. After 690 s the shutter was closed and the annealing process started. The smoothening of the film is indicated by the gradually increasing reflectivity. Above an annealing temperature of about 680 K, there is no further improvement. This treatment leads to well ordered films with a roughness of less than one monolayer as can be proved directly by reflectivity measurements. A detailed study of film growth by means of growth oscillations has been described in references 90, 92, 93.

For the case of Gd, the relation between growth parameter and magnetic properties has been studied in detail in reference [18], leading to a standard preparation method for Gd films that consists of film growth at room temperature with subsequent annealing to a temperature that depends on film thickness. Epitaxial growth of other heavy lanthanide metals, like Tb, Dy, and Ho, has been studied down to thicknesses of 70 Å (about 25 monolayers) [90, 94]. In the present work, all films were prepared with the substrate held at room temperature during deposition. The individual annealing temperatures of different metals and different thicknesses were obtained by reflectivity measurements during annealing as discussed in the example above. Ultrathin Ho films below 14 monolayers were prepared in two different ways, with annealing to 670 K and without annealing. While the annealed films show a slightly more pronounced magnetic diffraction pattern, no deviation in the systematics of parameters like magnetic period and magnetic ordering temperature could be observed. Films of Dy thicker than 100 Å were grown in two steps to achieve the best crystalline order. A seed layer of about 20 monolayers was grown and annealed, then the growth process was continued. The growth parameters are summarized in table 3.2.

The films prepared in this way are characterized by very high crystalline quality. The crystalline order of a sample is given by the mosaic spread of the lattice, which is measured by the width of the diffraction peaks along the corresponding direction in momentum space. For thin films, the number of coherently scattering planes can be determined from the shapes of the Bragg peaks by equation 2.6. A comparison of the number of layers and the total film thickness taken from reflectivity measurements of the films studied in the present work, reveals that almost the whole film is of single-crystalline order. The in-plane crystalline order is checked by rocking scans as displayed in the inset of figure 2.3. Typical rocking widths were of the order of 0.06°, which is comparable to very high-quality bulk single crystals.

Y/Ho/Y films

The second type of samples studied in this dissertation were *ex-situ* grown Ho films sandwiched between two Y layers. These films were grown in a standard way by means of molecular-beam epitaxy [64, 95, 96]. In these case, the substrate was an $a-$plane sapphire crystal with a Nb/Y buffer system to ensure epitaxial growth. The Y layer, with lattice constants similar to those of Ho, are meant to reduce epitaxial strain in the Ho layer. Furthermore, Nb acts as a chemical buffer to prevent reaction between the rare earth material (Y, Ho) and the sapphire. The samples were capped by Y/Nb layers to avoid oxidation when exposed to air. Additionally, the Nb oxide formed on the topmost Nb layer protects the sample from the diffusion of hydrogen into the bulk. The samples were grown in an MBE system in the group of Prof. Zabel at the Ruhr-Universität Bochum. X-ray reflectivity confirmed high sample quality with a rms-roughness of the Ho/Y interface of 2-3 monolayers.

Setups and facilities

The study of crystalline and magnetic structures of thin and ultrathin films by means of x-ray scattering is demanding. Structural studies require photon energies well above 5 keV, where the wavelength fits the crystalline lattice parameters. Usually such experiments are performed at photon energies around 10 keV. In this energy region, magnetic structures can be studied as well, but due to the comparably low magnetic-scattering signal, this method is not suitable for ultrathin films. By application of resonant magnetic soft x-ray scattering, the studies could be extended to this thickness region, as shown in this work. The different experiments in the two photon-energy regions require different experimental setups, which are discussed in the following.

The combined studies of crystalline and magnetic structures were done in the conventional x-ray region at the respective L_{III} absorption thresholds. The experiments were carried out at the ID10 A (Troïka) beamline of the *European Synchrotron Radiation Facility* (ESRF) in Grenoble, France [97]. The Troïka is an undulator beamline with x-ray-transparent diamond and beryllium transmission monochromators. For the experiments we used the diamond (111) reflex in asymmetric Laue geometry with an energy and angular

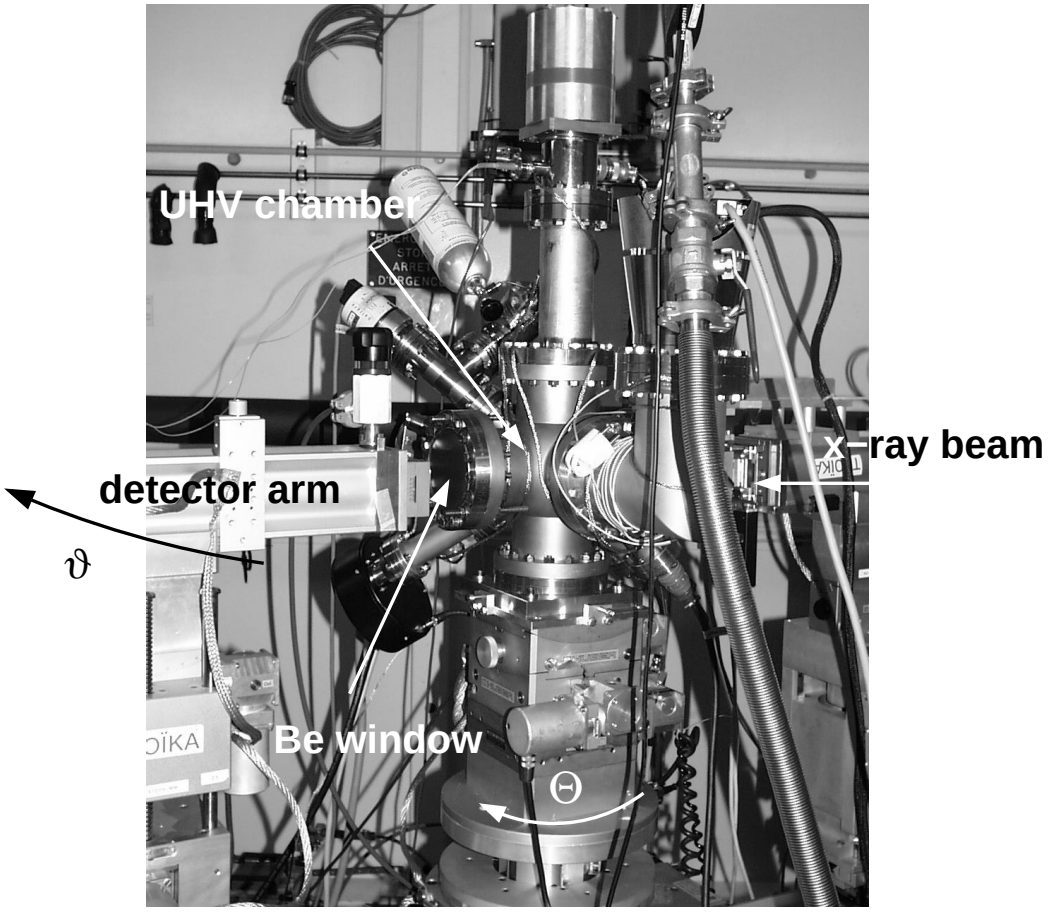

Figure 3.3: Experimental setup used at the ID10 A Troïka beamline at the ESRF.

acceptance of $\Delta\lambda/\lambda = 3.2 \cdot 10^{-5}$ and $\Delta\theta = 12.9\,\mu$rad at a photon energy of 8 keV. The beamline is equipped with a four-circle diffractometer, which can be operated in horizontal and vertical scattering geometry. A two-circle analyzer stage for polarization analysis is part of the diffractometer assembly. The experiments on Dy were performed in horizontal scattering geometry with π polarized incoming x-rays as shown schematically in figure 2.6. For polarization analysis of the scattered x-rays, which was needed to discriminate magnetic scattering from charge scattering, we used a graphite analyzer crystal. The different polarization states ($\pi\pi$ and $\pi\sigma$ channel) could be separately detected by rotating the analyzer crystal around the direction of observation (see discussion in section 2.2).

To prepare the samples *in situ,* it was necessary to mount a complete UHV setup onto the diffractometer at the beamline. Because of limitations in size and weight, we used a small chamber based on a CF-100 double cross, equipped with two Be windows of 0.5 mm thickness for the incident and reflected beam. This chamber is permanently pumped by a turbo-molecular pump backed by a turbo-molecular drag pump and a membrane pump to achieve a pressure in the low 10^{-11}-mbar range with the closed-cycle refrigerator for sample cooling in operation. The chamber was further equipped with evaporators and a

thickness monitor for sample preparation and a quadrupole mass spectrometer for residual gas analysis. A photograph of the chamber, mounted on the diffractometer, is shown in figure 3.3. The sample surface is oriented towards the backside of the setup. A detailed description of the Troïka beamline and the diffractometer can be found in reference 98.

The measurements of the lattice parameter of the MBE-grown Ho films were performed at the W1.1 wiggler beamline at the *Hamburger Synchrotronstrahlungslabor* (HASYLAB) [99]. A modified vacuum chamber was mounted to the beamline diffractometer in vertical scattering geometry. Instead of the Be windows as used in the setup at the ESRF a Be dome was used to achieve a 2Θ range of about 160°. In the used energy interval of 8-12 keV it was possible to reach the Ho(002) up to the (00 10) Bragg peaks. Furthermore, by using the Be dome, we could mount three samples in one run and change the samples simply by a translation of the whole chamber perpendicular to the scattering plane.

In the soft x-ray region, the experiments were performed at the U49/1-SGM, U49/2-PGM and UE52-SGM undulator beamlines at the *Berliner Elektronenspeicherring für Synchrotronsrahlung* (BESSY) [100]. Experiments with soft x-rays are particularly demanding for mainly two reasons. Firstly, the strong absorption of soft x-rays in air requires that both sample and detector must be inside a vacuum chamber connected directly to the beamline. Secondly, for the investigation of *in-situ* grown lanthanide-metal films it is necessary to provide very good UHV conditions as discussed in the previous section. This requires a diffractometer design with all motors outside the vacuum, since outgassing from the motors inside would limit the quality of the vacuum. Therefore, we designed and constructed a *two-circle in-situ* diffractometer as shown in figure 3.4. The sample motion is realized by a differentially-pumped rotary feed-through. Coaxial to the sample motion a detector rotation is installed. The detector motion is driven by a gearwheel through a high-resolution rotary feed-through. With this design, the motions could be realized with stepping motors outside the vacuum providing good UHV conditions (below $5 \cdot 10^{-11}$ mbar) even when the diffractometer is moving. The scattered intensity was recorded with a Si photodiode mounted behind a rectangular slit on the detector arm. The size of the detector slit can be changed between 50 μm and 2 mm by means of a rotatable slit carousel as can be seen on the photograph in figure 3.4. Most of the experiments were done with an 100 μm slit which defines the angular resolution to 0.05°. As it turned out, a polarization analysis is not required in the soft x-ray region for separating the magnetic signal from charge scattering. This setup could be either equipped with the same W(110) substrate crystal and evaporators as used in the setup at the ESRF, or with a second sample holder to investigate the MBE-grown samples. By that, complementary experiments in both energy regions on identical or identically-prepared samples could be performed.

Currently, there are only a few operating soft x-ray diffractometers in the world. Most of these instruments have more degrees of freedom for sample alignment than ours. But their high angular flexibility limits the coupling to the cryostat, and thus the cooling power. Also most of these instruments have been designed with motors running inside the vacuum. To my knowledge, there is presently no other diffractometer available, which combines true UHV conditions and effective sample cooling required for the experiments performed in this work.

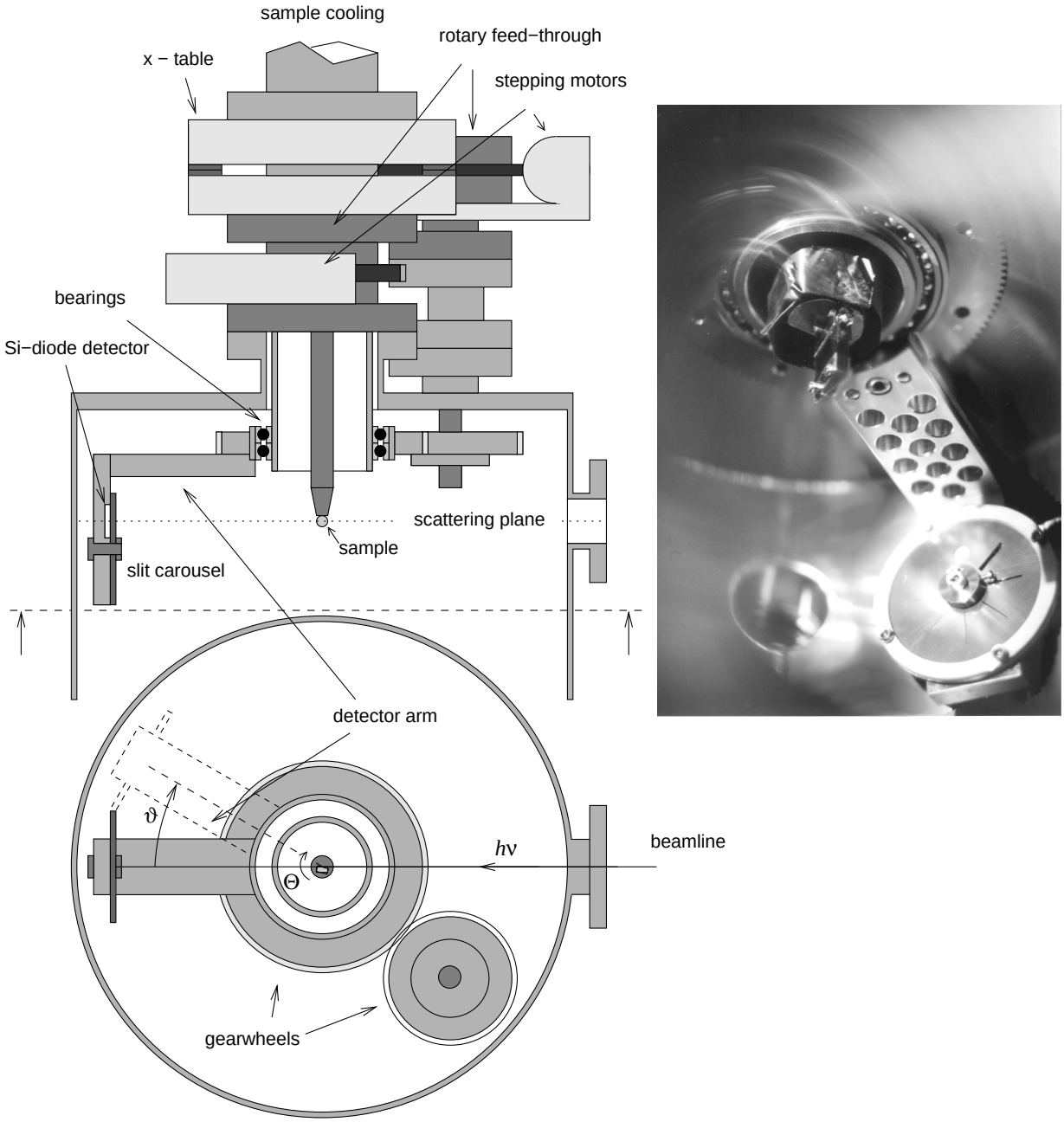

Figure 3.4: In-vacuum diffractometer built for scattering in the soft x-ray region. Left side: schematic drawing of the diffractometer inside the vacuum chamber. The upper part is a cross section of the vacuum chamber and the diffractometer perpendicular to the scattering plane. The lower drawing is a view from below onto the diffractometer. The photograph on the right side gives a view into the vacuum chamber showing the sample and the detector arm with the slit carousel.